
Title: Modelling and experimental investigation on textured surface generation in vibration-assisted micro-milling

Authors: Wanqun Chen, Lu Zheng, Wenkun Xie, KaiYang, Dehong Huo

PII: S0924-0136(18)30500-4
DOI: https://doi.org/10.1016/j.jmatprotec.2018.11.011
Reference: PROTEC 16004

To appear in: *Journal of Materials Processing Technology*

Received date: 14 May 2018
Revised date: 26 October 2018
Accepted date: 9 November 2018

Please cite this article as: Chen W, Zheng L, Xie W, KaiYang, Huo D, Modelling and experimental investigation on textured surface generation in vibration-assisted micro-milling, *Journal of Materials Processing Tech.* (2018), https://doi.org/10.1016/j.jmatprotec.2018.11.011

# Modelling and experimental investigation on textured surface generation in vibration-assisted micro-milling

Wanqun Chen[1,2], Lu Zheng[3], Wenkun Xie[2], KaiYang[4], Dehong Huo[3*]

[1]*EPSRC Future Metrology Hub, Centre for Precision Technologies, University of Huddersfield, Huddersfield, HD1 3DH, UK*

[2]*School of Mechatronics Engineering, Harbin Institute of Technology, Harbin 150001, P. R. China*

[3]*School of Engineering, Newcastle University, Newcastle upon Tyne, NE1 7RU, UK*

[4]*Army Aviation Institute, Beijing 101123, P. R. China*

[*]*Corresponding author: D. Huo, Tel: 44 (0) 191 208 6230, E-mail: dehong.huo@newcastle.ac.uk*

**Abstract:**

This paper investigates the textured surface generation mechanism in vibration-assisted micro milling through modelling and experimental approaches. To decouple the effects of tool geometry and kinematics of vibration-assisted milling, a surface generation model based on homogenous matrices transformation is proposed. On this basis, series of simulations are performed to provide insights into the effects of various vibration parameters (frequency, amplitude and phase difference) on the generation mechanism of typical textured surfaces in 1D and 2D vibration-assisted milling. Furthermore, the wettability tests are performed on the machined surfaces with various surface texture topographies. The fish-scale textured surfaces are found to exhibit better wettability than those with wavy-structure. The results indicate that vibration-assisted milling is an effective method to generate certain surface textures with controllable wettability.

**Keywords:** Vibration-assisted machining; micro-milling; vibration assisted milling; textured surface; surface generation modelling; wettability;

Nomenclature:

$r_e$-- corner radius ;
$r_b$ -- cutting edge radius
$k'$ -- angle of the minor cutting edge;
R -- tool radius;
ω -- angular velocity of the cutter;
$z_i$ -- $i^{th}$ cutter tooth;
Z -- number of flutes;
$v_f$ -- feed velocity;
A -- vibration amplitude in *x* direction;
B -- vibration amplitude in y direction;
$f_x$ --vibration frequency in x direction;
$f_y$ -- vibration frequency in y direction;
$\phi_x$ -- phase angle in x direction;
$\phi_y$ -- phase angle in y direction;
φ-- initial angle between $X_t$ and $X_T$ axes;
$t$ -- cutting time;
$\theta$ -- relative rotational angle;
$a_e$-- radial cutting depth;
$i$ -- number of feed in cross-feed direction;
D—tool diameter;

## 1. Introduction:

The functional surface with periodic micro/nanostructures, owing to its excellent abilities, such as reducing adhesion friction, improving lubricity and specific optical properties (Jung and Bhushan, 2006; Liao et al., 2000; Maboudian, 1997; Judy, 2001), have found wide applications in optics, automotive, aerospace, biomedical, and power generation devices (Hadad and Ramezani, 2016; Wilkinson et al., 1997). The reseach, development and innovation of novel cost-effective machining method for special functional surface has become one research hot across the world.

Vibration-assisted machining, as one kind of machining strategy capable of generating specific surface texture more conveniently, has been proposed. Using elliptical vibration-assisted turning, Brehl, Dow. (2008) and Sajjady et al. (2016) succeed in fabricating micro structure. Moreover, it was found that vibration could be helpful to reduce surface roughness. Similarly, various kinds of vibration-assisted machining methods including vibration-assisted EDM, vibration turning, etc., have been proven to be feasible for fabricating various mico/nanoscale surface patterns. Owing to its excellent machining performance, vibration-assisted machining has attracts more-and-more attention of researchers.

Recently, vibration-assisted milling, as one typical vibration machining method, has been found to be capable of conveniently generating surface micro-structure (Uhlmann et al. (2015). By adopting resonable vibration paramters (such as vibation frequence, amplitude, etc.) and machinining parameters, desirable surface texture with specific micro/nanoscale topography could be obtained (Tong et al., 2018; Kim and Loh, 2011; Suzuki et al., 2007, 2011). For instance, Börner et al. (2018) found that special micro-structure can be generated repeatedly by considering the cutting conditions such as kinematics and cutting edge geometry. Chen et al. (2018a) investigated the trajectories of tool tips in non-resonant vibration-assisted milling and proposed a method for generating two specific types of surface textures (wave and fish scale) by combining different vibration and machining parameters. Overall, vibration-assisted milling (VAMILL), due to high machining efficiency, low cost and simple machine equipment setup, has been proven to be one cost-effective machining strategy for fabricating textured surface with special functional surface. However, in the state of the art, very little attention is given to 2D vibration assisted milling processes, due to the complexity of kinematics and dynamics of this process. Ding et al. (2010) investigated the machinability improvement of hardened tool steel using two-dimensional vibration-assisted micro-end-milling and found that it was an effective method to machine hardened tool steel and can be applied in the manufacture of moulds and dies with improved machining efficiency, surface quality and tool life. Chen et al. (2018b) investigated the tool-workpiece separation mechanism of 2D assisted milling process. Three typical types of tool-workpiece separation were proposed and the requirements to realize each type of separations were obtained.

There are many factors affect the surface generation, such as tool geometry parameters (Wojciechowski et al., 2018a), machining parameters (Wojciechowski et al., 2018b, Chen et al., 2018), machining stability (Nieslony et al., 2018), especially for vibration assistant milling, the surface texture generation process, is very complicated. Any change in processing parameters could result in significant change of the processed microstructure. To obtain high-performance surface texture, it is very important to study the influence of different machining and vibration parameters on surface generation (Ehmann and Hong, 1994). For this reason, many numerical simulation-based efforts have been devoted to predicting the surface

generation in conventional milling, micro milling or VAMILL. A time domain end milling process simulation was performed by Peigné et al. (2003) and a 2.5-D geometrical modelling milled surface was proposed. By employing kinematic rules and transformation operators, Kouravand and Imani. (2014) established a micro-channel surface texture model for micro milling process to consider the effects of minimum chip thickness and the geometrical features of cutting edge, and the surface texture generation process was simulated by using a 3D B-rep geometric kernel as geometric engine. Vakondios et al. (2014) developed a surface simulation model for ball milling process, and it was integrated in a commercial CAD software, however, it was difficult to read numerical information, as the surface textures were generated in a solid mode. Ding et al. (2011) proposed a numerical modelling method for VAMILL process using a dexel-like calculation algorithm. In this model, although the tool profile was mapped along tool path to consider the effects of multiple tool engagements on surface generation, the effects of the tool geometry was still overlooked. Tao et al. (2017) also analyzed the influence of tool parameters on surface generation, they simplified the tool cutting edge as a sharp one, to simple the simulation process and reduce the computation time, but it reduces the accuracy of the surface texture simulation. Recently, Börner et al. (2018) proposed an improved modelling model for textured surface generation in VAMILL. By a dexel-based data model to describe workpiece and tool, actual tool geometry can be considered in the modelling of textured surface generation, this method can improve the simulation accuracy by using small discrete distance, however, its time-consuming. Up to date, there are still many problems in current simulation methods, such as low simulation accuracy and complicated calculation procedures. A simulation method for VAMILL satisfied both simple and accuracy is desperately needed. In addition, the effects of machining parameters and vibration parameters on the textured surface generation are still not clear understood, and it has become a significant technical obstacle preventing the extensive use of special functional surface in creating innovative products by VAMILL.

For these reasons, this paper proposed an accurate modelling method (verified by VAMILL experiments) to predict the surface topography in VAMILL process to consider the effects of cutting edge radius, machining kinematics and coordinate transformation. The proposed method could realize the surface modelling with any tool geometry and complex machining trajectory. Compared with the previous model, the actual cutting edge equation is adopted, which will improve the model accuracy, and reduce the time-.Based on this novel modeling method, the generation mechanism of structured surface in vibration assisted milling, especially the correlation among machining/vibration parameters, surface texture and its wettability, could be determined.

The paper can be divided into distinct sections. Section 2 gives the details of the modeling method of the generation of surface topography in vibration assisted milling process. Then, the proposed modelling method is verified by machining experiments to in Section 3. Moreover, in Section 4, the effects of the vibration parameters on the surface wettability and the tool wear in the vibration assisted milling process are analyzed and discussed. At last, Section 5 summarizes the main conclusions based on the present work.

## 2. Surface generation modeling in vibration assisted milling

The generation process of textured surface can be recognized as the result of the

interactions between a cutter with a specific shape and workpiece. In the machining process, the cutter is fed at specified machining path, and surface microstructures could be formed on the machined surface due to the cutting edge overlap trajectories. Thus, the surface generation in vibration-assisted milling is easily affected by various factors, including the kinematics of machining systems, the real geometry of cutting edge, machining and vibration parameters, etc. To accurately model the vibration-assisted milling surface generation process, the cutting edge detection and modelling, the kinemics modeling and analysis, and the coordinate transformation from cutting edge to workpiece surface, are the key steps.

As illustrated in Fig.1, one HMT-based calculation algorithm for the surface generation of VAMILL is proposed and it mainly consists of the following steps:

Firstly, the geometry of the cutting edge is detected by scanning electron microscope (SEM) and atomic force microscope (AFM), and it can be described with a numerical function. Secondly, the cutting edge and workpiece are discretized into series of points. Thirdly, all points on the cutting edge are transferred from tool coordinate system to workpiece coordinate system by HMT, which forms the simulated surface in a point cloud. Then the Z-map technology, which means plot the minimum *z* as a function of *x* and *y* in the workpiece coordinate system, is applied to generate the final machined surface.

### 2.1 Cutting edge modelling

To accurately predict the surface topography in the vibration assisted milling process, the real contour of the cutting edge should be first described. Thus the micro end mills were first detected by SEM and AFM before machining experiments to obtain the cutter geometry parameters. Figs.2 a) and b) give the SEM images for the side and top views of micro milling tool. And the angle of minor cutting edge is measured in one analysis software ImageJ®. Besides, the cutting edge radius is detected by AFM, and it is further determined obtained by using the least squares fit method, as illustrated in Fig.2 c). The detailed geometrical parameters of the micro cutting tool are summarized in Table 1.

The profile of cutting edge, which is shown in Fig.2 d), can be described as:

$$z = f(x) = \begin{cases} -x\tan k + (R - r_e - r_e\sin k)\tan k + r_e(1-\cos k), & 0 < x < R - r_e - r_e\sin k \\ -\sqrt{r_e^2 - \left[x - (R - r_e)\right]^2} + r_e, & x \geq R - r_e - r_e\sin k \end{cases} \quad (1)$$

where $r_e, k'$, and R denote the corner radius, angle of minor cutting edge, and tool radius, respectively. The tool center, as shown in Fig.2d) is set to the origin of coordinate system, *Z* axis is aligned with the tool axis, and XY-plane is aligned with the tool rake face of one cutting flute.

### 2.2 Kinemics analysis of vibration assisted milling

To realize the oscillating motion between the cutting tool and workpiece in the VAMILL process, there are two choices: tool or workpiece for superimposing the high frequency small amplitude vibration and in this paper, workpiece is selected. As shown in Fig.3, workpiece is simultaneously fed in *x*- and *y*-direction, and the axial depth of cut is in *z* direction.

The relative displacement ($x_i$, $y_i$) of tool tip to workpiece in VAMILL can be depicted by Eq.(2):

$$\begin{cases} x_i = v_f t + R\sin\left[\omega t - \dfrac{2\pi(z_i - 1)}{Z}\right] + A\sin\left(f_x t + \phi_x\right) \\ y_i = R\cos\left[\omega t - \dfrac{2\pi(z_i - 1)}{Z}\right] + B\sin\left(f_y t + \phi_y\right) \end{cases} \tag{2}$$

where $R$ and $\omega$ are the radius and angular velocity of the cutter, $z_i$ is the $i^{th}$ cutter tooth, and $Z$ is number of flutes. $v_f$ is feed velocity. $A$ and $B$ are the vibration amplitudes, $f_x$ and $f_y$ are the vibration frequencies, $\phi_x$ and $\phi_y$ are the phase angles, in $x$- and $y$-directions.

### 2.3 Homogeneous matrix transformation

From Eq.(2), it can be noted that except for $t$, 10 independent parameters are required to determine the tool tip trajectory in the 2D vibration-assisted milling. Owing to the effects of so many parameters, the tool tip trajectory in VAMILL is much more complex. In order to accurately describe the tool tip trajectory in VAMILL, the homogeneous matrix transformation (HMT) method (Ehmann and Hong, 1994; Peigné et al., 2003) is adopted and the detailed HMT process in VAMILL are introduced in the following section.

#### 2.3.1 HMT in VAMILL

It is widely recognized that the surface topography of machined surface can be generated by the cutting of the cutting edge on the workpiece. Therefore, the HMT of the VAMILL should be conducted for the whole cutting edge, the tool tip trajectory can be obtained by using this method.

Fig.4 shows the equipment setup schematic diagram for the vibration-assisted milling. The removal of workpiece material is performed by the cutter with high rotation speed. In the workpiece, the vibration is applied on the workpiece, and the workpiece is fed along $x$-direction. Also, it can be seen that the local coordinate system of the cutter ($O_t$-$X_tY_tZ_t$) and the rotation coordinate system ($O_T$-$X_TY_TZ_T$) are applied to describe the tool profile and the spindle rotation. Besides, the translation coordinate systems, i.e. $O_V$-$X_VY_VZ_V$ and $O_W$-$X_WY_WZ_W$ are used to depict the vibration on the workpiece and the feed of the control system. The detailed transformation or rotation values of each coordinate system in the VAMILL process are given in Table 2.

The homogeneous coordinates of the cutting edge in $O_t$-$X_tY_tZ_t$ is given as:

$$\begin{bmatrix} x_t \\ y_t \\ z_t \\ 1 \end{bmatrix} = \begin{bmatrix} x \\ 0 \\ f(x) \\ 1 \end{bmatrix} \tag{3}$$

The $O_T$-$X_TY_TZ_T$ only considers the rotation speed of the cutter. The $X_T$ and $Y_T$ axis are aligned with the cutter feed and cross-feed directions, respectively. The $Z_T$ axis is parallel to $Z_t$. The origin of the two coordinates (tool coordinate system and local tool coordinate system) is at the same point. Therefore, the spindle angular velocity can be considered as the angular velocity

of $O_t$-$X_tY_tZ_t$ with respect to $O_T$-$X_TY_TZ_T$. As time goes by, the relative rotational angle ($\theta$) of two coordinate systems change the position which is shown in Fig.5. When the points of the cutting edge are changed from $O_t$-$X_tY_tZ_t$ to $O_T$-$X_TY_TZ_T$, the rotational effect is considered.

$$\theta = \varphi - \omega t \tag{4}$$

where $\varphi$ is the initial angle between $X_t$ and $X_T$ axes. In this paper, it is set to 0°. $\omega$ is the tool rotation angular velocity *(rad/s)* and $t$ is cutting time *(s)*.

The homogeneous transformation matrix (HTM) from $O_t$-$X_tY_tZ_t$ to $O_T$-$X_TY_TZ_T$ can be expressed as:

$${}^{T}T_{t} = \begin{bmatrix} \cos\theta & -\sin\theta & 0 & 0 \\ \sin\theta & \cos\theta & 0 & 0 \\ 0 & 0 & 1 & 0 \\ 0 & 0 & 0 & 1 \end{bmatrix} \tag{5}$$

In the workpiece coordinate system ($O_W$-$X_WY_WZ_W$), $X_W$, and $Y_W$, refer to the feed direction and cross-feed direction, respectively. And $Z_W$ represents the direction of the axial cutting depth, which is parallel to $Z_t$. In 3-axis milling process, only the translation between $O_W$-$X_WY_WZ_W$ and $O_T$-$X_TY_TZ_T$ occurs. According to the actual machining situation, the initial relative position of $O_W$-$X_WY_WZ_W$ to $O_T$-$X_TY_TZ_T$ could be determined.

By transforming the coordinates of the tool cutting edge from $O_t$-$X_tY_tZ_t$ to $O_W$-$X_WY_WZ_W$, the relative position of each point on the cutting edge to workpiece can be obtained, and the height of the cutting edge at any point could also be recorded through $Z_W$ coordinate.

The original coordinate of $O_T$-$X_TY_TZ_T$ for each feed in cross-feed direction relative to $O_W$-$X_WY_WZ_W$ is obtained by:

$$\begin{cases} x_{0T} = x_0 + (i-1)a_e \\ y_{0T} = y_0 + v_f t \\ z_{0T} = z_0 \end{cases} \tag{6}$$

where $(x_0,y_0,z_0)$ is the initial position of the origin of $O_T$-$X_TY_TZ_T$ in the $O_W$-$X_WY_WZ_W$, and it is set as *(0,-R,0)* in this paper. $a_e$ is radial cutting depth *(mm)*. $i$ is the number of feed in cross-feed direction; $v_f$ is the feed speed in $Y_w$ direction *(mm/s)*.

As shown in Fig.2, owing to the effect of the vibration applied on the workpiece, the relative displacement between tool and workpiece is changed. Thus, the origin coordinates of $O_T$-$X_TY_TZ_T$ for each feed in radial direction relative to the origin of $O_W$-$X_WY_WZ_W$ can be calculated as:

$$\begin{cases} x_{0T} = x_0 + (i-1)a_e + A\sin(2\pi f_x t + \phi_x) \\ y_{0T} = y_0 + v_f t + B\sin(2\pi f_y t + \phi_y) \\ z_{0T} = z_0 \end{cases} \tag{7}$$

where *x(t)* and *y(t)* denote the components of the dynamic instantaneous displacement between tool and workpiece in *x*-and *y*-direction, respectively.

Thus, the HTM from $O_T$-$X_TY_TZ_T$ to $O_W$-$X_WY_WZ_W$ can be expressed as:

$$ {}^{W}T_{T} = \begin{bmatrix} 1 & 0 & 0 & x_0 + (i-1)a_e + A\sin(2\pi f_x t + \phi_x) \\ 0 & 1 & 0 & y_0 + v_f t + B\sin(2\pi f_y t + \phi_y) \\ 0 & 0 & 1 & z_0 \\ 0 & 0 & 0 & 1 \end{bmatrix} \tag{8} $$

The cutting edge in the workpiece coordinate system $O_W$-$X_WY_WZ_W$ can be expressed as:

$$ \begin{bmatrix} x_W \\ y_W \\ z_W \\ 1 \end{bmatrix} = {}^{W}T_{T}\,{}^{T}T_{t} \begin{bmatrix} x_t \\ y_t \\ z_t \\ 1 \end{bmatrix} = \begin{bmatrix} x\cos\theta + x_0 + (i-1)a_e + A\sin(\omega t + \phi) \\ x\sin\theta + y_0 + v_f t + B\sin(\omega t + \phi) \\ f(x) + z_0 \\ 1 \end{bmatrix} \tag{9} $$

By using above HMT method, two typical tool tip trajectories in VAMILL are shown in Fig.6. When the ratio of vibration frequency to spindle rotation frequency (RVS) is odd, a complex surface texture is generated by overlapping of adjacent cuter teeth. Differently, for even RVS, a wavy surface is formed. The difference in surface topographies at different RVSs clearly indicates that the RVS has significant influence on surface texture generation. Thus, in the following study, the RVS is considered as one key factor for optimal selection of machining and vibration parameters.

**2.3.2 Surface generation**

According to the copy principle of tool contour, the workpiece surface topography is formed by sweeping of the cutting edge profile along the tool path. In order to numerically simulate surface generation, tool cutting edge and workpiece are discretized into a series of elements. Then the surface topography of the machined surface could be formed by mapping the cutting edge contour onto workpiece surface. Following above procedures, as illustrated in Fig.7, the cutting edge is discretized into numerous elements, and workpiece is evenly divided into *n* columns and *m* rows. Each row and column intersect, forming one grid point. The height of each point on the machined surface of the workpiece can be obtained by calculating the tool cutting depth (*z*-coordinate) at grid point. To obtain one complete surface, the height of middle position between two grid points can be obtained by a curve fitting algorithm.

**2.4 Surface generation simulation**

Surface simulation is an effective way for in-depth understanding of the vibration-assisted milling process of structured surface, which is significant to realize the deterministic manufacturing of functional surface. Therefore, in this section, serials of surface generation simulations are performed to elucidate the underlying relationship among machining and vibration parameters, surface texture and its wettability.

In those simulations, two assumptions are given: The tool diameter significantly exceeds the length of the milled tracks and the tool will not be deflected in the feed direction, therefore, the re-cutting effect can be neglected in the present work.

The machining parameters and cutter parameters (such as spindle rotation speed, number of tooth and the feed per teeth) are pre-defined, as shown in Table 3. In our previous investigation (Chen et al. 2018a), RVS and vibration amplitude were found to significantly affect surface texture generation. Thus, in this study, eight typical sets of vibration parameters are selected. The spindle speed is kept at 6,000rpm (rotation frequency is 100Hz). The vibration frequency is set as 8300 Hz (odd number to spindle rotation frequency) and 8400 Hz (even number to spindle rotation frequency). Meanwhile, three typical vibration amplitudes, that is, 2, 5 and 7μm, are employed. They are less, equal and larger than the half of the feed rate (10 μm per tooth), respectively. In addition, to study the influence of phase difference between the two vibration directions on the surface generation, the phase difference is set to 0, $\pi/4$ and $\pi/2$, respectively.

It can be found from set 1-3 (see Table 3), that the vibration frequency applied in *x*-direction is an odd times of spindle rotation frequency. Since the vibration applied is a sinusoidal-based signal, the valleys (crests) of the current cutter path intersect with the crests (valleys) of the following cutter trajectory. Consequently, three types of surface topographies are obtained, as shown in Fig.8 a-c). Different kinds of fish squamous topographies are produced on the machined surface, respectively corresponding to those vibration amplitudes that are less, equal and larger than half of the feed per tooth.

In the vibration-assisted milling experiments of Set 4, since the vibration frequency applied in *x*-direction is even times of the spindle rotation frequency, the crests (valleys) of the current cutter path are intersected with those of the following cutter trajectory, thereby forming a wavy surface, as shown in Fig.8 d).

In the vibration-assisted milling experiments of set 5 and 6, vibration are applied in *x*- and *y*- directions. The vibration frequencies are even times of the spindle rotation frequency, with the phase difference between two vibration signals is $\pi/2$ and zero. Under the combined effects of *x*- and *y*-direction vibrations, it can be seen in Fig.8 e) and f) that the crests (valleys) of the current cutter path also meets those of the following cutter trajectory. Meanwhile, due to the phase difference between two vibration signals, the spatial distribution of the wavy surface is also changed, as shown in Fig.8 e) and f).

Finally, though *x*- and *y*-direction vibrations are also applied in in the milling experiments of Set 7 and 8, the vibration frequencies (odd times of spindle rotation frequency) and the phase differences of zero and $\pi/2$ are adopted. ). At those vibration parameters, it can be noted from Fig.8 g) and h) that the valleys (crests) of the current cutter path meet the crests (valleys) of the following cutter trajectory. Finally, two evidently-different surfaces topographies are obtained, which should be also attributed to the effects of different phase differences between two vibration signals.

## 3. Vibration-assisted milling experiments

In the present work, all of milling experiments were conducted on a 3-axis precision milling machine tool (NANOWAVE MTS5R) equipped with a 2D vibration platform on the Z-direction machine slideway, as illustrated in Fig.9a). The layout of the vibration stage control system is shown in Fig. 9b). The piezo actuators are driven by control signal, which is set by a host computer and then amplified by a high voltage piezo amplifier. Meanwhile, the vibration

displacement data of the platform is detected by two high precision capacitive sensors (CS005, Micro-epsilon) and collected by data acquisition cards, then sent back to the host computer for recording. The accuracy of vibration platform will be unavoidably influenced by many factors, including manufacturing errors, displacement coupling and control signal distortion, etc.

For verifying the vibration trajectory errors of the designed vibration platform, two sets of voltage input signals with same parameters (0.2 V, 1000 Hz) but different phases (90°) are sent to the piezo actuators in two directions. The testing results are shown in Fig.9c) . It can be noted that the total vibration trajectory error of the platform is 0.25 μm, meeting the requirements of micro-milling experiments.

To verify above simulation results, same machining parameters are adopted, as illustrated in Table.4. The uncoated double-edged micro tool is adopted, and the detailed geometry parameters of the tool can be found in Table.1. In order to ensure the relevance of the used data, an easy to machine material Al 6061 is used, and small axial depth of cut of 15μm were adopted in this study to avoid the effects of the self-excited vibration and rapid tool wear on the machined surface topography.

The surface topography of each machined surfaces is tested by a white light interferometer surface profilometer (Vecco NT1100), as shown in Fig.10. From the comparation of the profile and geometric size of the surface texture, it can be clearly found that Figs.10 a), b), and d) agree well with the simulation results (see Fig.8 a), b) and d)), respectively. However, other experimental results are not consistent with the simulation results in Fig.8. It should be ascribed to the effects of different kinds of vibrations. In the milling experiments corresponding to Fig.10 a), b) and d), the vibration is only applied in one direction. The control of vibration amplitude is easy. However, in the milling experiments corresponding to Fig.10 e-h), vibration is applied in both of *x*-and *y*-directions. Owing to the stiffness coupling effect of 2D-vibration stage, namely, the interaction effect of the *x*- and *y*-direction vibrations, vibration amplitude and the phase difference between *x*- and *y*-direction vibration signals do not reach the expected value. As for the milling corresponding to Fig.10 c), the overlap of two adjacent cutting edges is too small to be reflected on the machined surface, due to the elastic recovery of the material in the material removing process. As the material properties of the workpiece are not considered in current simulation model, the height profile of the milling surface is larger than the simulated surface.

Overall, the surface texture model proposed in the present work could accurately describe the surface generation in 1D vibration-assisted milling process. The proposed surface modelling method is based on homogenous matrices transformation and the cutter geometry, and not tool diameter dependent. Although micro milling experiments were used in this paper, the method is applicable to a conventional milling process. However, due to the couple effect of *x*- and *y*-direction vibration, it is still hard to accurately predict the surface generation in 2D vibration assisted milling process.

## 4. Discussion and analysis

The water contact angle on each machined surface is measured by a Sindatek Water Contact Goniometer with 5 ml water droplets. From Fig.10, it can be also clearly found that

the workpiece surface generated at different vibration parameters exhibit different wettability. According to the measured water contact angles, the wettability of fish scale surface is evidently better than that of wavy structure. The practical contact angle can be controlled from 30° to 89° by changing the vibration parameters. Therefore, the vibration-assisted milling is absolutely feasible to obtain the machined surface with controllable wettability, which could be realized by only adjusting the vibration parameters in the milling process.

**4.1 The influence of vibration parameters on surface wettability**

To quantitatively analyze the influence of vibration frequency, amplitude and phase difference on the surface wettability of the machined surface, new sets of the experiments have been conducted and surface contact angles were measured.

Fig.11 plots the contact angle versus vibration frequency and amplitude in the feed direction vibration condition. When the vibration frequency is 8400Hz, wavy texture is generated on the surface. But it has little effect on surface wettability, the contact angle only changes from 84° to 87°. When the vibration frequency changes to 8300Hz, odd multiples of the spindle rotation frequency, fish squamous structure are generated on the surface. Different from wavy texture, the fish squamous structure is found to be able to significantly increase hydrophilicity. At different vibration amplitudes, the contact angle of the machined surface changes from 30° to 89°. As shown in Fig.11, the contact angle decreases with the increase of the vibration amplitude and reaches the lowest point when the vibration amplitude (5 μm) equal with the half of the feed per tooth (10 μm). After that, the contact angle tends to increase with vibration amplitude.

Fig.12 illustrates the effects of phase difference and vibration frequency on the contact angle when the vibration applied in the feed and cross feed direction.

When the vibration frequency is 8400Hz (even multiples of spindle rotation frequency), the contact angle increases to 89° at phase difference of $\pi/4$. Then the contact angle tends to reduce to the lowest point ( about 73°) at the phase difference of $\pi/2$. After that, though the contact angle is slightly increased, it is still less than the contact angle of the surface generated without vibration.

When the vibration frequency changes to 8300Hz (odd multiples of the spindle rotation frequency), complex surface topography is generated on the machined surface, reducing the contact angle of the machined surface. As shown in Fig.12, the contact angle tends to decrease with the increase of the phase difference, it reaches the lowest point of about 53° when the phase difference is $\pi/2$. After that, the contact angle is also slightly increased with the vibration amplitude, but it is still less than that of the surface generated without vibration.

**4.2 Tool wear analysis**

The influence of the vibration frequency on the tool wear is investigated. The tool wear in the machining process with same feed-direction but different vibration frequency is compared. Two vibration frequencies of 8400 Hz and 8300 Hz, namely, even and odd multiples of the spindle rotation frequency (100 Hz), are adopted. After machining 30×20 mm slots, it can be

noted from Fig. 13, both of the corner radius and minor cutting edge of the tool are damaged. It should be due to the fact that when the vibration frequency is odd multiples of the spindle rotation frequency, the valleys (crests) of the current cutter path meet the crests (valleys) of the following cutter trajectory. Consequently, the instantaneous cutting thickness changes drastically, resulting intermittent impact on tool. When the vibration frequency is even multiples of the spindle rotation frequency, differently, the valleys (crests) of the current cutter path meet the valleys (crests) of the following cutter trajectory. In such case, no sudden change in instantaneous cutting thickness occurs and the cutting force changes smoothly. So slight worn of the corner radius and minor cutting edge of the tool could be found, as shown in Fig.14. Based on above analysis, it can be noted that the RVS not only affects the surface texture generation, but also has great influence on tool wear. When the fish-scale surface texture is generated, the wear rate of tool is faster, compared with that of wavy-structure.

**4.3 Potential application**

The functional surfaces with controllable surface wettability have exhibited wide applications in many fields. For instance, in micro-channel, such kind of functional surface enables to effectively control the flow rates and mixing efficiencies of different fluids on the specific region of micro-channel, significantly contributing to enhance the functional performance the micro-channel device. However, it is difficult to achieve controllable surface wettability in different regions of micro-channel by traditional processing methods, which requires novel promising machining process capable of solving this key issues. In the present work, vibration-assisted milling has been proven to be one viable solution for such type of application. By combining modeling and experiments, the surface generation mechanism of textured surface in vibration assisted machining has been emphatically focuses, which is significant to the further application of vibration-assisted machining in the fabrication of such kind of functional surface. The proposed surface work well for 1D vibration-assisted milling, but it is still not accurate enough to predict the generation of surface topography in 2D vibration-assisted machining, due to the coupling effect of *x*- and *y*-direction vibrations. Besides, it should be noted that, in this study, the back-cutting effect is neglected. Nevertheless, for a long slot machining, the back-cutting effects should be fully considered. Though it is beneficial to reduce surface roughness, no obvious texture could be generated on the multi-cut surface, due to the effects of the minimum cutting thickness and material elastic recovery. This phenomenon

limits the processing of microstructures using vibration assisted milling. A novel machining strategy should be further investigated to avoid the back-cutting effect in the future.

## 5 Conclusion

In this paper, based on the homogeneous matrix transformation and cutting-edge sweeping technology, a surface topography modelling model for vibration-assisted micro milling is proposed. On the basis, the influence of the machining and vibration parameters on surface texture generation and wettability performance are investigated. The following conclusions can be drawn:

1. A simple and accurate surface generation model is proposed, emphatically focusing on the effects of vibration parameters on the surface generation mechanism. The proposed surface texture model could accurately depict the generation process of surface topography in 1D vibration-assisted milling.
2. The ratio of vibration frequency to spindle rotation frequency (RVS) has significant influence on the surface texture generation. Periodical fish scale textured surface can be generated, when the vibration frequency of 8300Hz applied in feed direction is odd multiple of the spindle rotation frequency. Wavy surface textures can be generated when the vibration frequency of 8400Hz applied in feed direction is even multiple of the spindle rotation frequency.
3. The vibration frequency has significant impact on tool wear, worse tool wear is found of 8300 Hz (odd multiples of the spindle rotation frequency) than 8400 Hz (even multiples of the spindle rotation frequency) because of instantaneous cutting thickness changes drastically.
4. The spatial distribution of the surface texture tends to change with the phase difference between *x*- and *y*-direction vibrations signals, and different textures can be generated by using different vibration parameters.
5. The relationship between the machining and vibration parameters and the contact angle is established. Machined surface wettability is controllable by changing the vibration parameters, the contact angle can be changes from 30° to 89°. Moreover, fish scale textured surface shows better wettability than wave structure.

## Acknowledgment

The authors gratefully acknowledge financial support of the National Natural Science Foundation of China (Grant No.51505107), the Engineering and Physical Sciences Research Council (EP/M020657/1) and Project (HIT.NSRIF.2017029) supported by Natural Scientific Research Innovation Foundation in Harbin Institute of Technology.

### Conflict of interest

The authors declare that there is no conflict of interest.

## Reference

Börner, R., Winkler, S., Junge, T., Titsch, C., Schubert, A., Drossel, W.G., 2018. Generation of functional surfaces by using a simulation tool for surface prediction and micro structuring of cold-working steel with ultrasonic vibration assisted face milling. J. Mater. Process. Technol. 255, 749–759. https://doi.org/10.1016/j.jmatprotec.2018.01.027

Brehl, D.E., Dow, T.A., 2008. Review of vibration-assisted machining. Precis. Eng. https://doi.org/10.1016/j.precisioneng.2007.08.003

Chen, W., Zheng, L., Huo, D., 2018. Surface texture formation by non-resonant vibration assisted micro milling. Journal of Micromechanics and Microengineering. 28, 025006.

Chen, W., Huo, D., Hale, J., Ding, H., 2018. Kinematics and tool-workpiece separation analysis of vibration assisted milling. International Journal of Mechanical Sciences, 136, 169-178.

Chen, Y., Li, H., Hou, L., Wang, J. and Bu, X., 2018. An Intelligent Chatter Detection Method Based on EEMD and Feature Selection with Multi-channel Vibration Signals. *Measurement*.

Ding, H., Ibrahim, R., Cheng, K. and Chen, S.J., 2010. Experimental study on machinability improvement of hardened tool steel using two dimensional vibration-assisted micro-end-milling. *International Journal of Machine Tools and Manufacture*, *50*(12), 1115-1118.

Ding, H., Chen, S.J., Cheng, K., 2011. Dynamic surface generation modeling of two-dimensional vibration-assisted micro-end-milling. Int. J. Adv. Manuf. Technol. 53, 1075–1079. https://doi.org/10.1007/s00170-010-2903-0

E. Uhlmann, I. Perfilov, D.O., 2015. Two-axis vibration system for targeted influencing of micro-milling.

Ehmann, K.F., Hong, M.S., 1994. A Generalized Model of the Surface Generation Process in Metal Cutting. CIRP Ann. - Manuf. Technol. 43, 483–486. https://doi.org/10.1016/S0007-8506(07)62258-6

Eng, D., Vakondios, D., Eng, D., Efstathiou, C., 2014. Cad-based simulation and surface topomorphy prediction in ball-end milling 1, 140–144.

Hadad, M., Ramezani, M., 2016. Modeling and analysis of a novel approach in machining and structuring of flat surfaces using face milling process. Int. J. Mach. Tools Manuf. 105, 32–44. https://doi.org/10.1016/j.ijmachtools.2016.03.005

Judy, J.W., 2001. Microelectromechanical systems ( MEMS ): fabrication , design and. Smart Mater. Struct. 10, 1115–1134. https://doi.org/10.1088/0964-1726/10/6/301

Jung, Y.C., Bhushan, B., 2006. Contact angle, adhesion and friction properties of micro-and nanopatterned polymers for superhydrophobicity. Nanotechnology 17, 4970–4980. https://doi.org/10.1088/0957-4484/17/19/033

Kim, G.D., Loh, B.G., 2011. Direct machining of micro patterns on nickel alloy and mold steel by vibration assisted cutting. Int. J. Precis. Eng. Manuf. 12, 583–588. https://doi.org/10.1007/s12541-011-0075-y

Kouravand, S., Imani, B.M., 2014. Developing a surface roughness model for end-milling of micro-channel. Mach. Sci. Technol. 18, 299–321. https://doi.org/10.1080/10910344.2014.897846

Liao, H., Normand, B., Coddet, C., 2000. Influence of coating microstructure on the abrasive wear resistance of WC/Co cermet coatings. Surf. Coatings Technol. 124, 235–242. https://doi.org/10.1016/S0257-8972(99)00653-2

Maboudian, R., 1997. Critical Review: Adhesion in surface micromechanical structures. J. Vac.

Sci. Technol. B Microelectron. Nanom. Struct. 15, 1. https://doi.org/10.1116/1.589247

Nieslony, P., Krolczyk, G.M., Wojciechowski, S., Chudy, R., Zak, K. and Maruda, R.W., 2018. Surface quality and topographic inspection of variable compliance part after precise turning. *Applied Surface Science*, *434*, pp.91-101.

Peigné, G., Paris, H., Brissaud, D., 2003. A model of milled surface generation for time domain simulation of high-speed cutting. Proc. Inst. Mech. Eng. Part B J. Eng. Manuf. 217, 919–930. https://doi.org/10.1243/09544050360686798

Sajjady, S.A., Nouri Hossein Abadi, H., Amini, S., Nosouhi, R., 2016. Analytical and experimental study of topography of surface texture in ultrasonic vibration assisted turning. Mater. Des. 93, 311–323. https://doi.org/10.1016/j.matdes.2015.12.119

Suzuki, N., Haritani, M., Yang, J., Hino, R., Shamoto, E., 2007. Elliptical vibration cutting of tungsten alloy molds for optical glass parts. CIRP Ann. - Manuf. Technol. 56, 127–130. https://doi.org/10.1016/j.cirp.2007.05.032

Suzuki, N., Yokoi, H., Shamoto, E., 2011. Micro/nano sculpturing of hardened steel by controlling vibration amplitude in elliptical vibration cutting. Precis. Eng. 35, 44–50. https://doi.org/10.1016/j.precisioneng.2010.09.006

Tao, G., Ma, C., Bai, L., Shen, X., Zhang, J., 2017. Feed-direction ultrasonic vibration−assisted milling surface texture formation. Mater. Manuf. Process. 32, 193–198. https://doi.org/10.1080/10426914.2016.1198029

Tong, H., Li, Y., Wang, Y., 2008. Experimental research on vibration assisted EDM of micro-structures with non-circular cross-section. J. Mater. Process. Technol. 208, 289–298. https://doi.org/10.1016/j.jmatprotec.2007.12.126

Wilkinson, P., Reuben, R.L., Jones, J.D.C., Barton, J.S., Hand, D.P., Carolan, T.A., Kidd, S.R., 1997. Surface finish parameters as diagnostics of tool wear in face milling. Wear 205, 47–54. https://doi.org/10.1016/S0043-1648(96)07253-5

Wojciechowski, S., Maruda, R.W., Krolczyk, G.M. and Niesłony, P., 2018. Application of signal to noise ratio and grey relational analysis to minimize forces and vibrations during precise ball end milling. *Precision Engineering*, *51*, pp.582-596.

Wojciechowski, S., Maruda, R.W., Barrans, S., Nieslony, P. and Krolczyk, G.M., 2017. Optimisation of machining parameters during ball end milling of hardened steel with various surface inclinations. *Measurement*, *111*, pp.18-28.

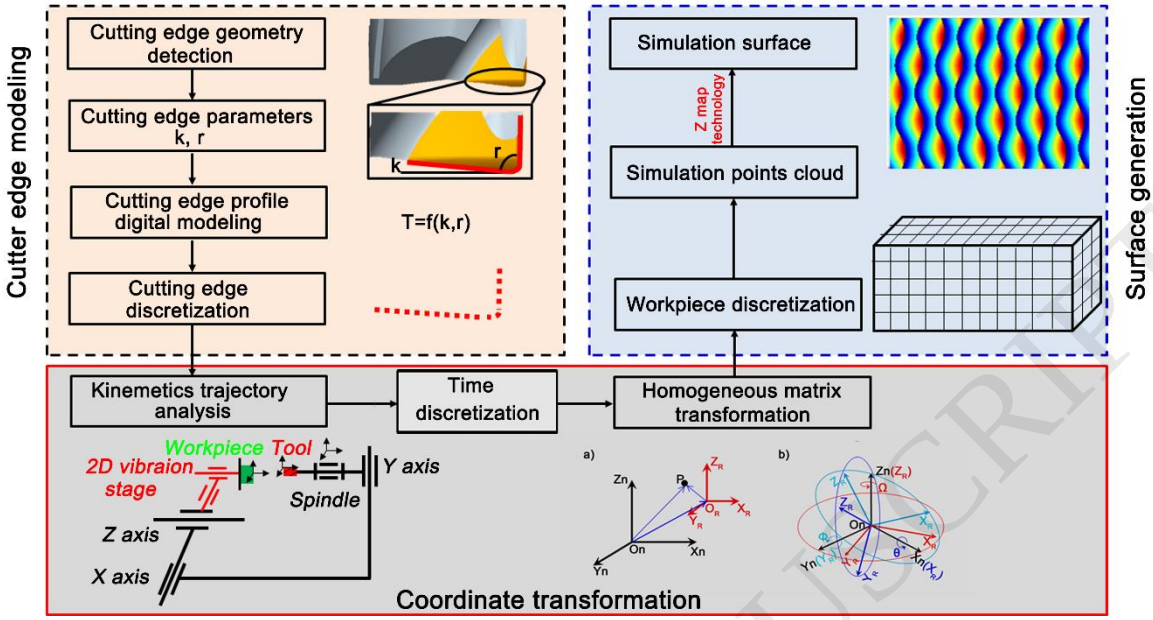


*Fig.1 Flow chart of the surface simulation process*

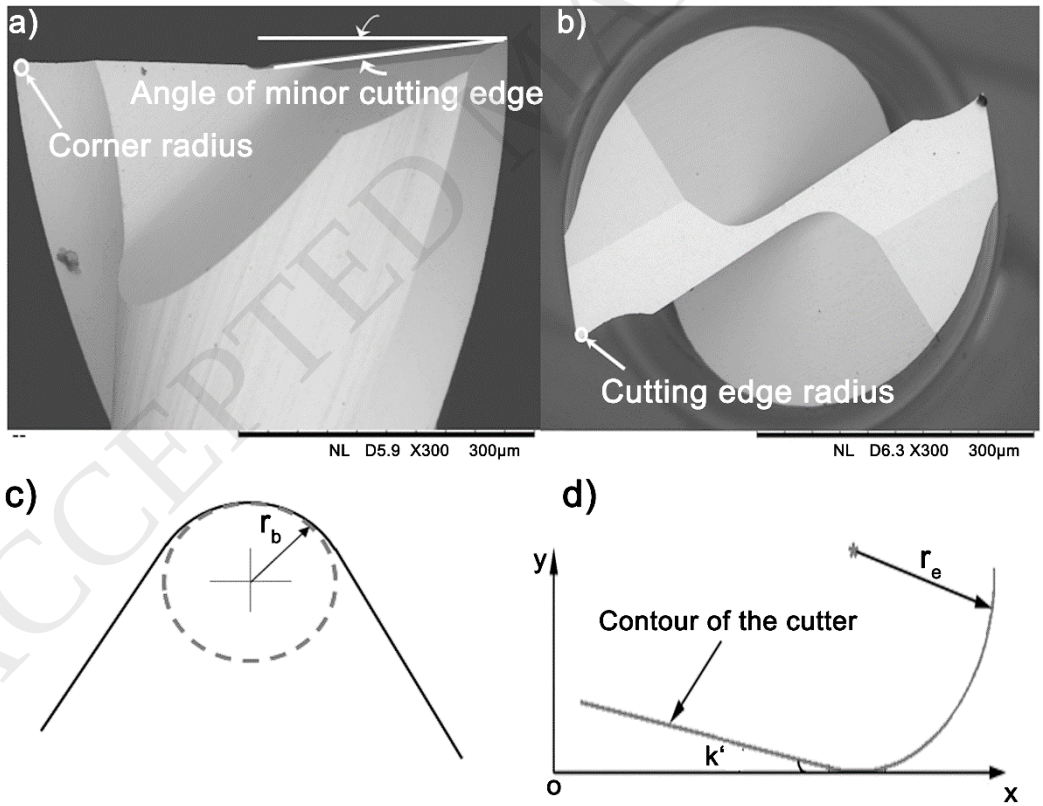


*Fig.2 Tool geometry. a) side view; b) top view; c) cutting edge radius fitting; d) end cutting edge profile.*

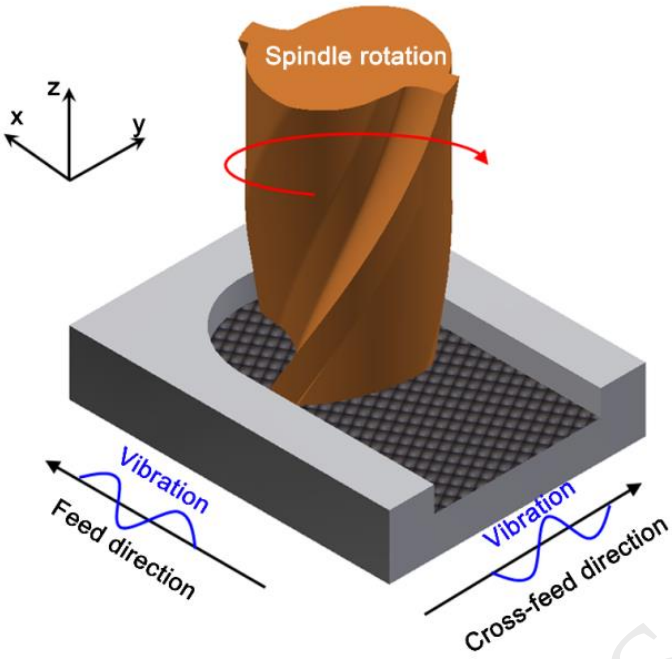


*Fig. 3 Schematic diagram of vibration assisted milling*

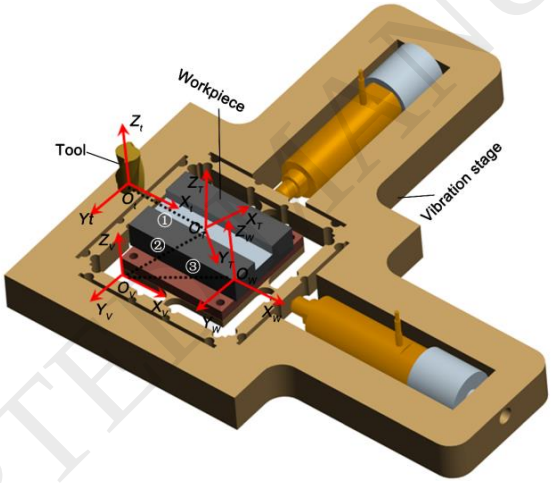


*Fig.4 Coordinate systems in vibration assisted milling*

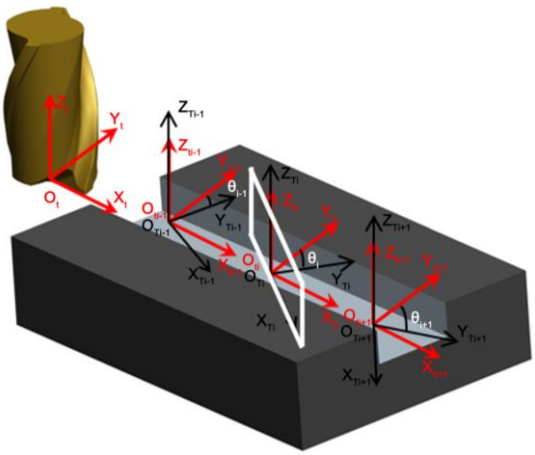

*Fig.5 Tool instantaneous attitude position*

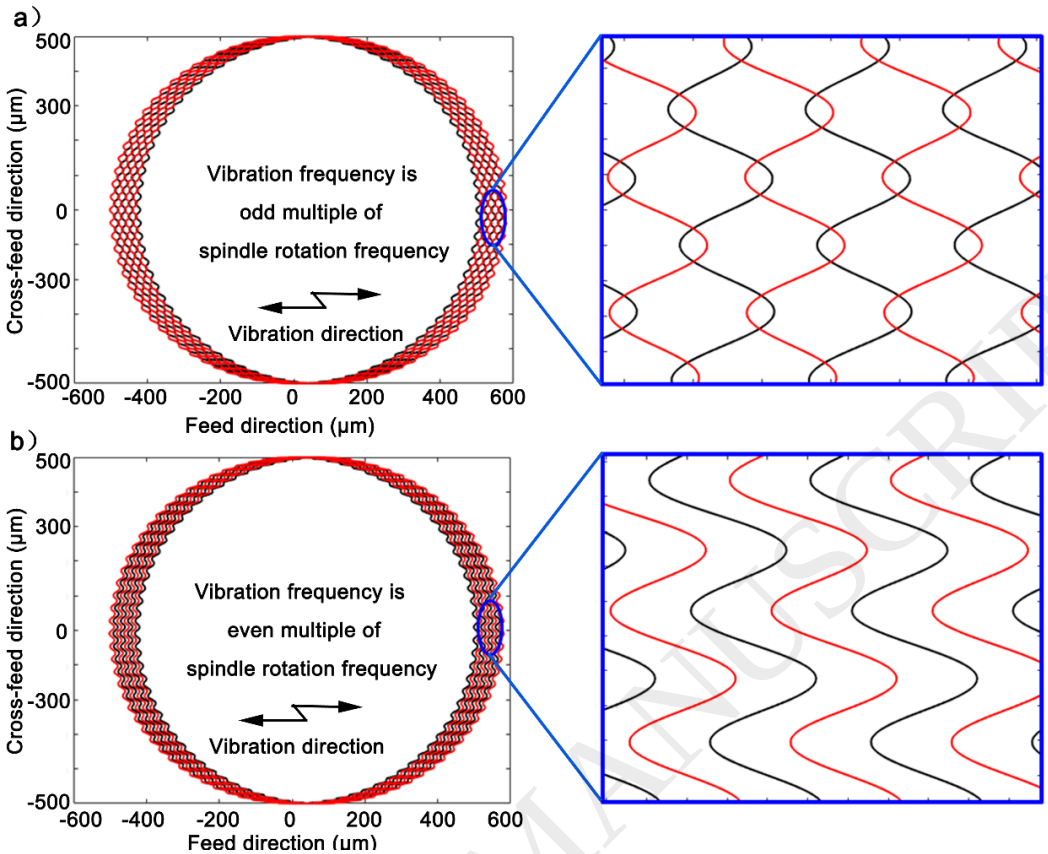


*Fig.6 Tool tip trajectories of VAMILL with different RVSs. a) Odd multiple, b) Even multiple*

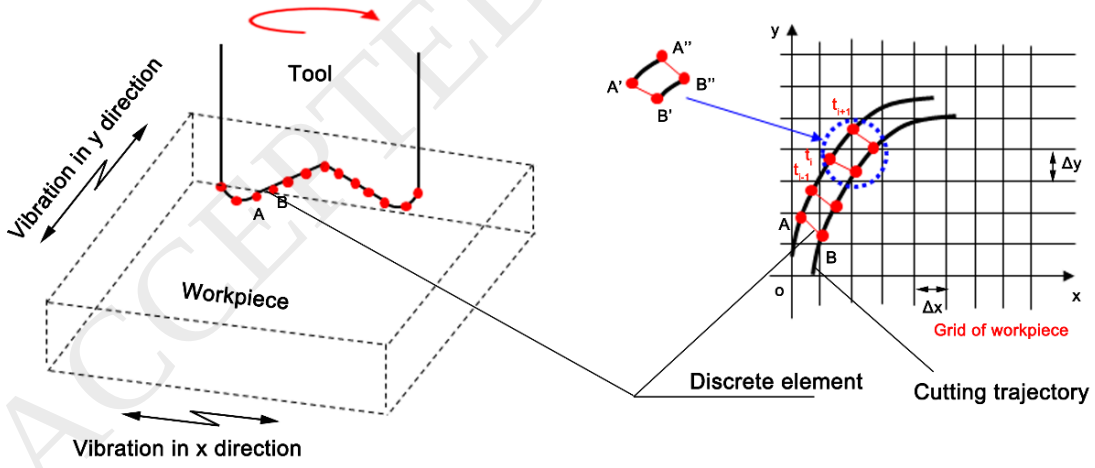


*Fig.7 Schematic of surface generation simulation algorithm*

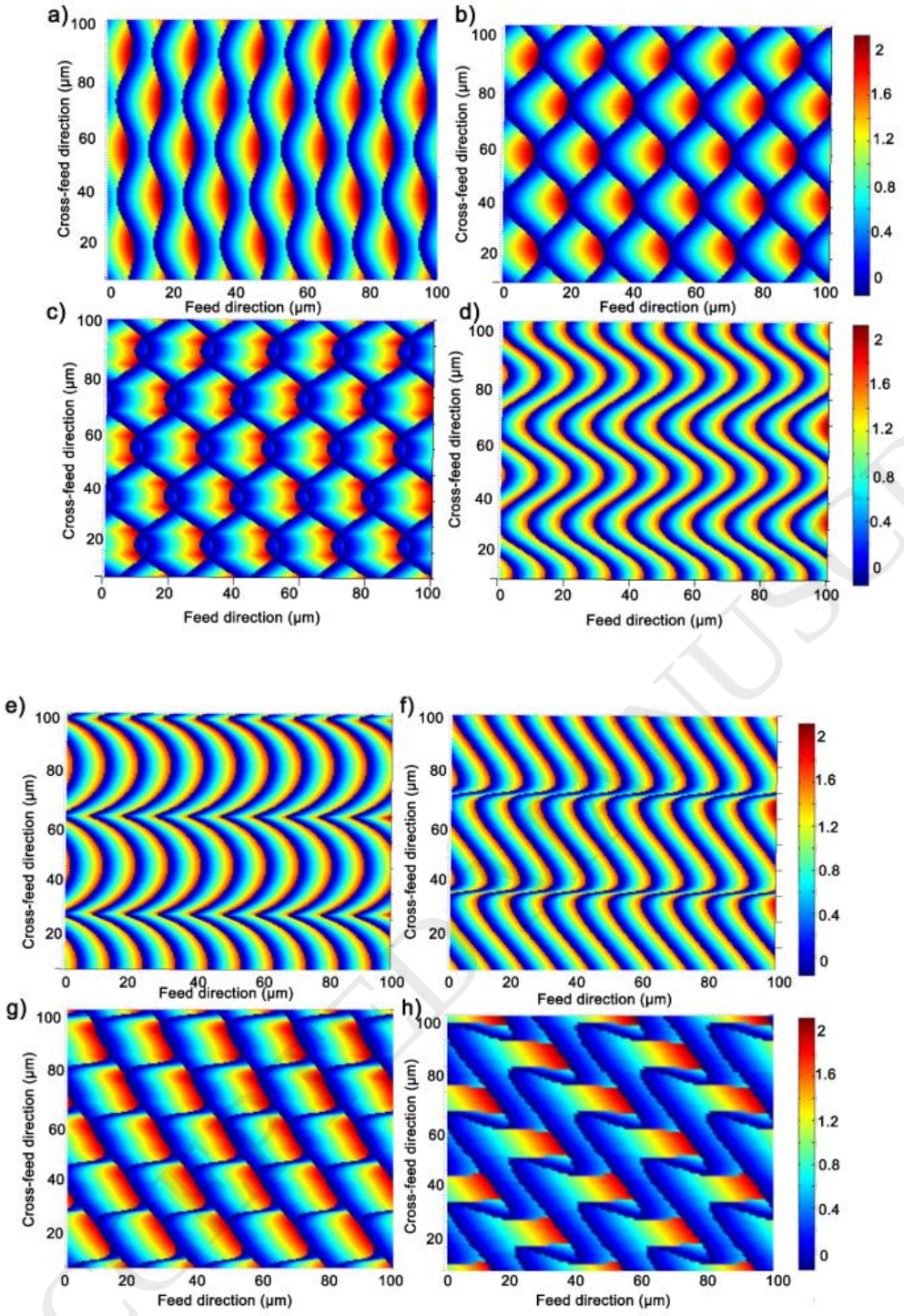


*Fig.8 Simulation results of the VAM surface. a-h) Surface generated with the machining and vibration parameters of set 1-8.*

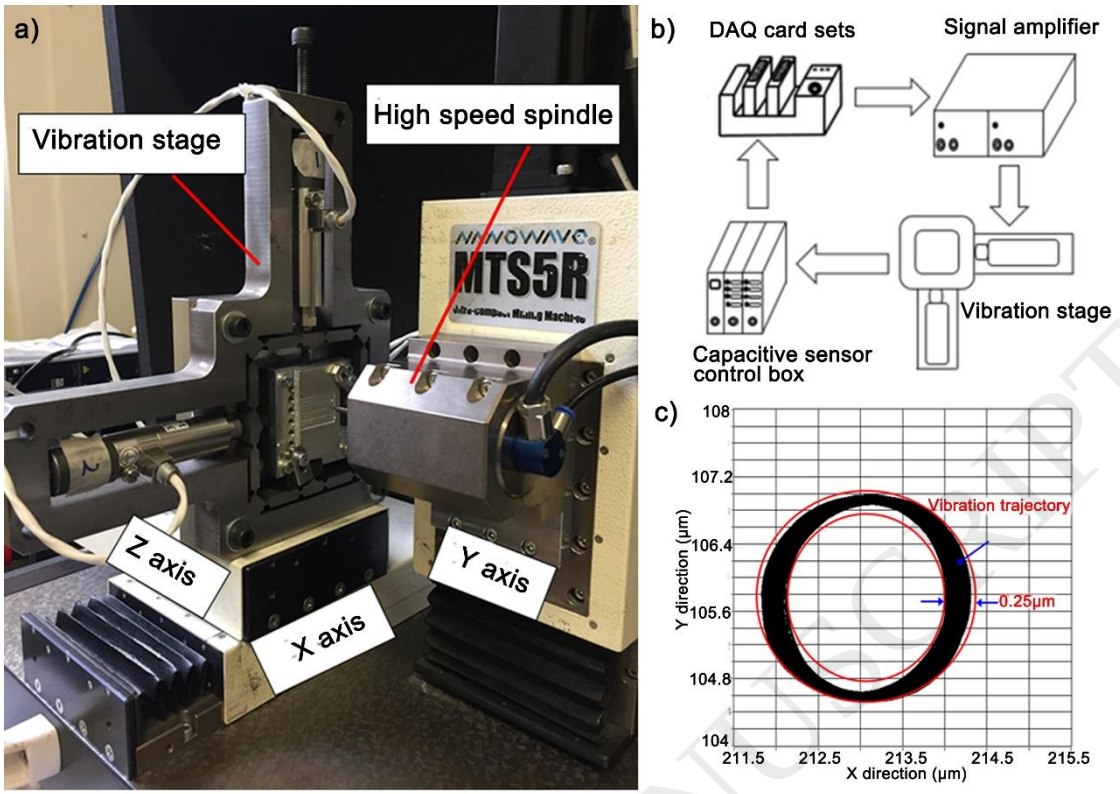


*Fig.9 Layout of VAMILL equipment. a) vibration assisted milling system; b) schematic of the vibration stage control system; c) error test result of the vibration stage*

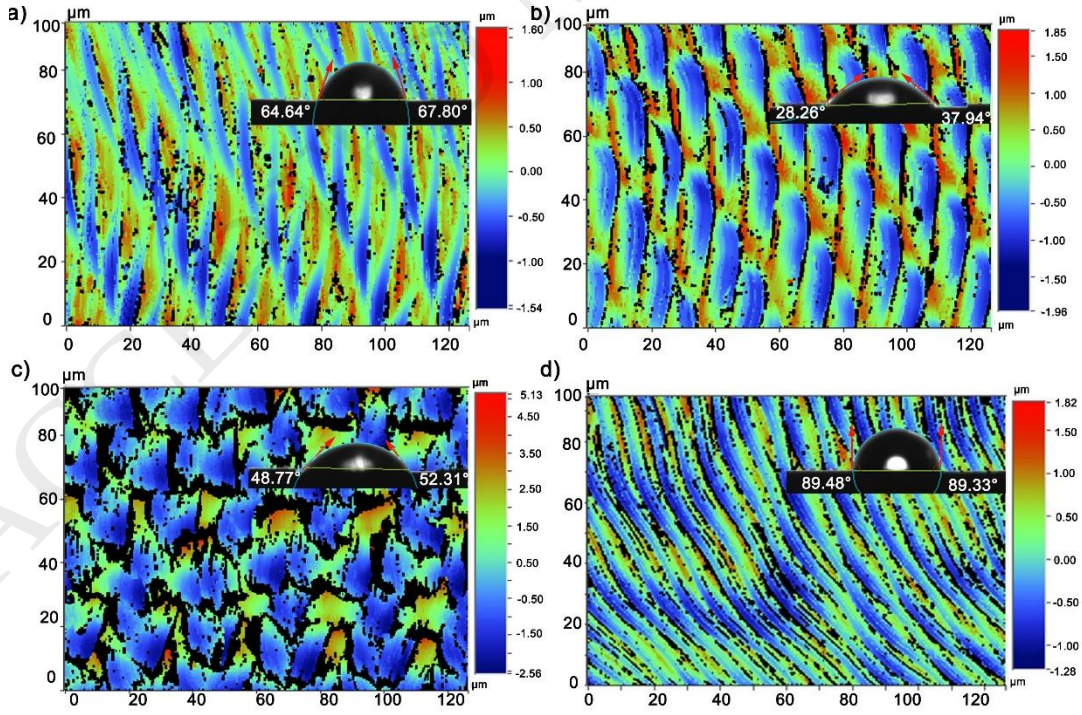

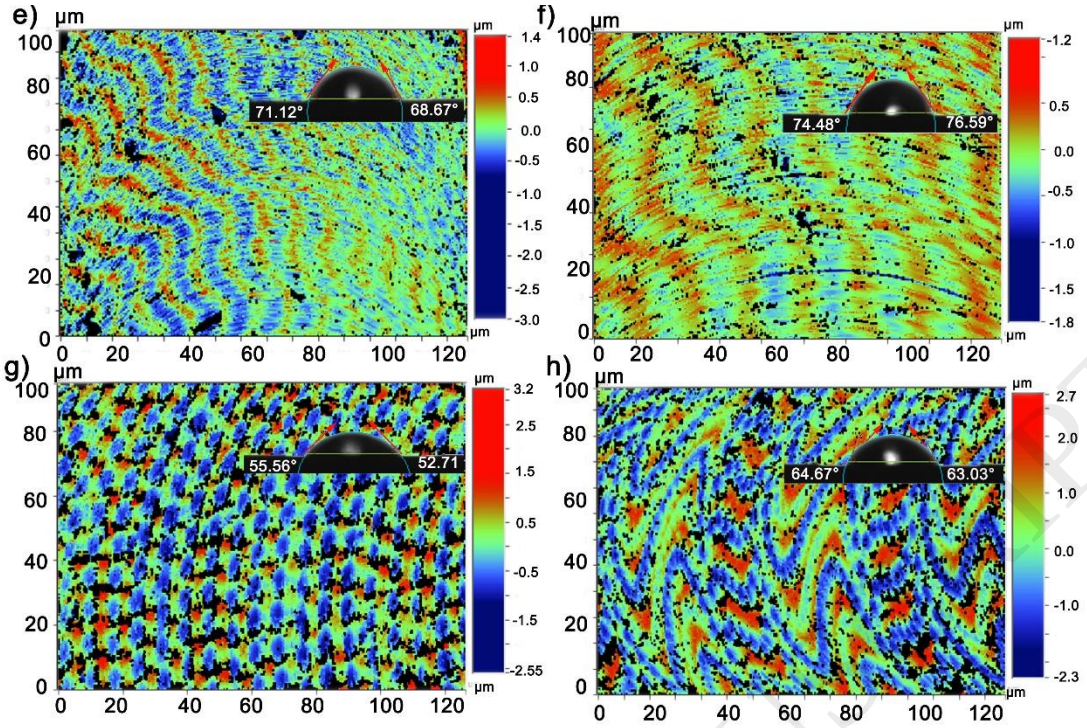


*Fig.10 Experiment results of the VAM surface. a-h) Surface generated with the machining and vibration parameters of set 1-8.*

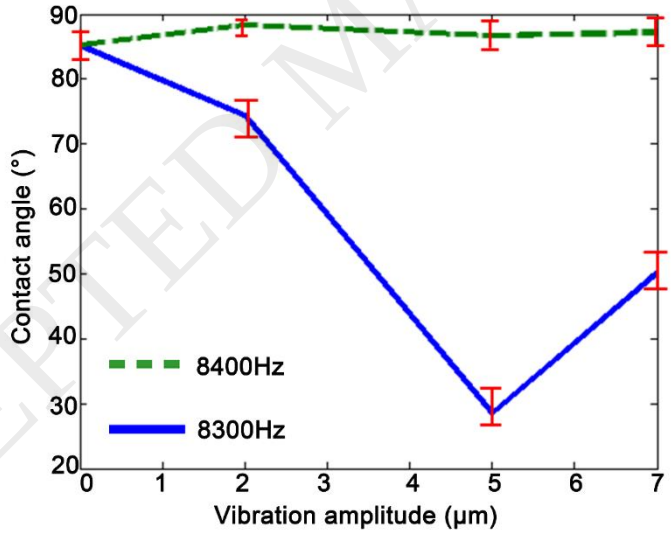


*Fig.11 Influence of the vibration frequency and amplitude on the contact angle*

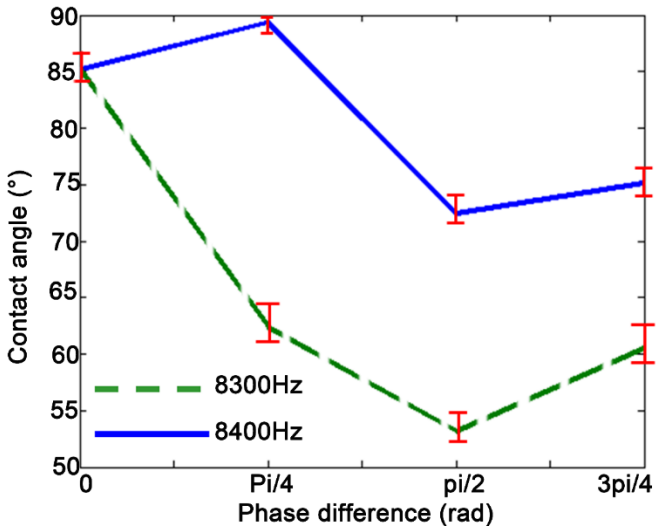


*Fig.12 The influence of the phase difference and vibration frequency on the contact angle*

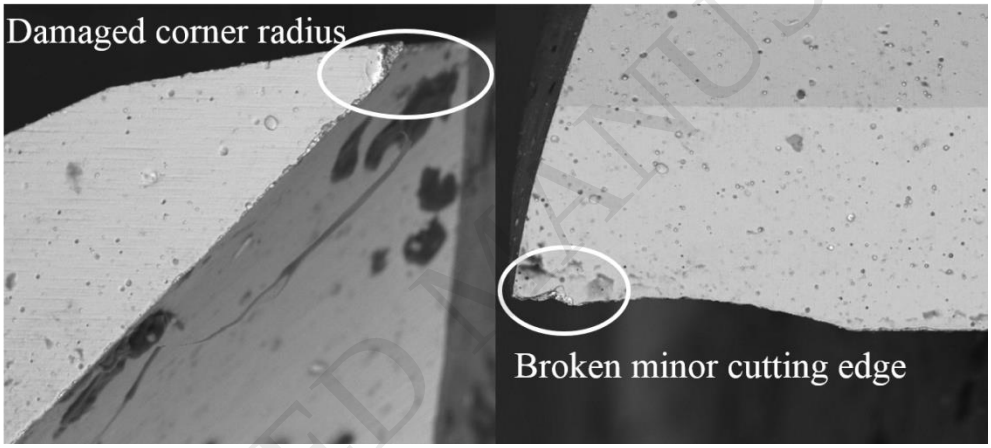


*Fig.13 Tool wear for fish scale generation*

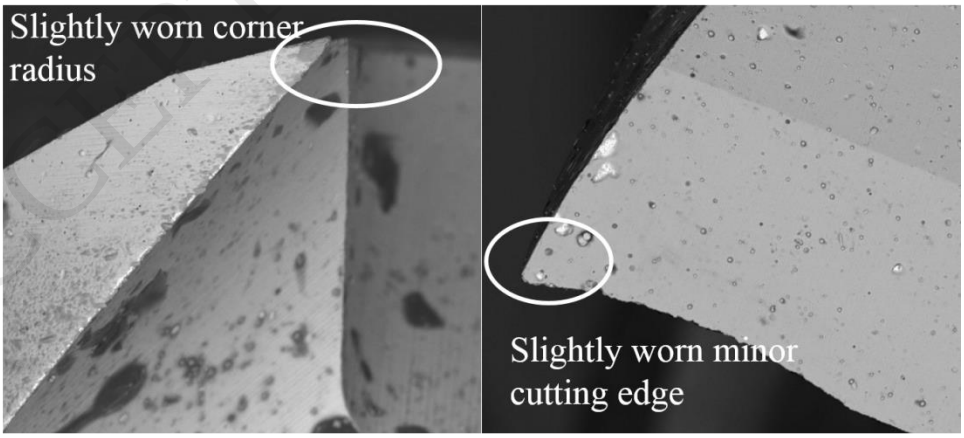


*Fig.14 Tool wear for wave surface generation*

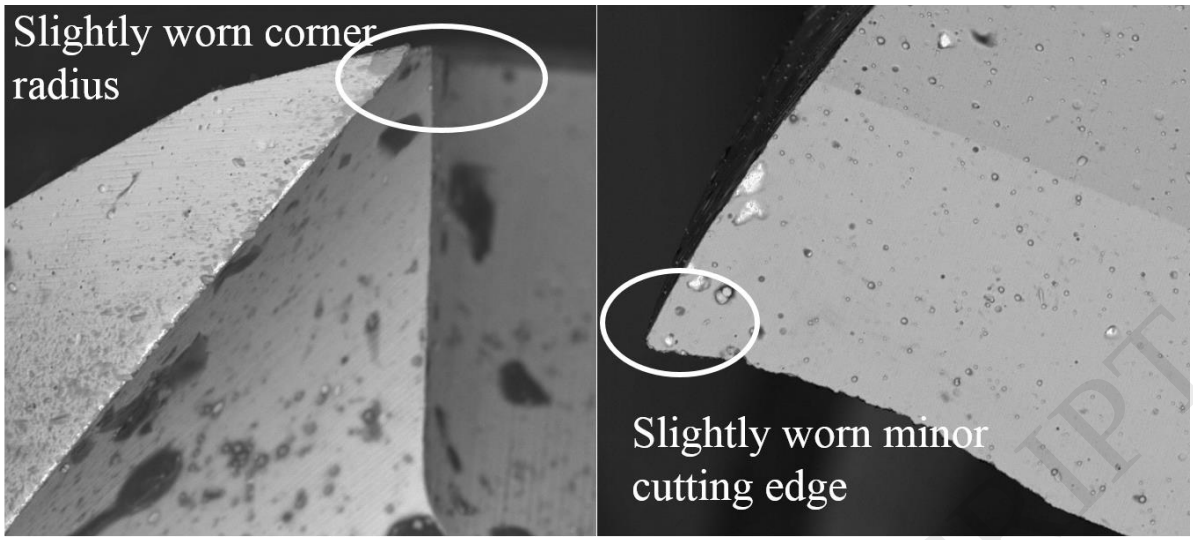


Fig 15

Table 1 Parameters of the micro cutting tool

| Parameter | Value |
|---|---|
| Tool diameter, $D$ | 1 mm |
| Number of flutes, $N$ | 2 |
| Corner radius, $r_e$ | 3 μm |
| Angle of the minor cutting edge, $k$ | 5° |
| Cutting edge radius, $r_b$ | 5μm |

Table 2 State value for each HMT

| HMT | $x$ | $y$ | $z$ | $\alpha$ | $\beta$ | $\gamma$ |
|---|---|---|---|---|---|---|
| ${}^{T}T_t$ | 0 | 0 | 0 | 0 | 0 | $\varphi - \omega t$ |
| ${}^{V}T_T$ | $A\sin(2\pi f_x t + \emptyset_x)$ | $B\sin(2\pi f_y t + \emptyset_y)$ | 0 | 0 | 0 | 0 |
| ${}^{W}T_V$ | $x_0 + (i-1)a_e$ | $y_0 + v_f t$ | 0 | 0 | 0 | 0 |

Table 3 Machining and vibration parameters

| Set No. | Spindle speed (rpm) | Feed per tooth (μm) | $x$-direction | | $y$-direction | | Phase difference (rad) |
|---|---|---|---|---|---|---|---|
| | | | vibration amplitude (μm) | vibration frequency (Hz) | vibration amplitude (μm) | vibration frequency (Hz) | |
| 1 | 6000 | 10 | 2 | 8300 | 0 | 0 | 0 |
| 2 | 6000 | 10 | 5 | 8300 | 0 | 0 | 0 |
| 3 | 6000 | 10 | 7 | 8300 | 0 | 0 | 0 |
| 4 | 6000 | 10 | 7 | 8400 | 0 | 0 | 0 |
| 5 | 6000 | 10 | 5 | 8400 | 5 | 8400 | π/2 |
| 6 | 6000 | 10 | 5 | 8400 | 5 | 8400 | 0 |

| | | | | | | | |
|---|---|---|---|---|---|---|---|
| 7 | 6000 | 10 | 5 | 8300 | 5 | 8300 | 0 |
| 8 | 6000 | 10 | 5 | 8300 | 5 | 8300 | $\pi/4$ |